Low-carbon Economic Dispatch of Integrated Energy Systems Considering Extended Carbon Emission Flow

Yumin Zhang, Pengkai Sun, Xingquan Ji, Fushuan Wen, Ming Yang, and Pingfeng Ye

Abstract—**Carbon capture and storage (CCS) systems can provide sufficient carbon raw materials for power-to-gas (P2G) systems to reduce the carbon emission of traditional coal-fired units, which helps to achieve low-carbon dispatch of integrated energy systems (IESs). In this study, an extended carbon-emission flow model that integrates CCS-P2G coordinated operation and low-carbon characteristics of an energy storage system (ESS) is proposed. On the energy supply side, the coupling relationship between CCS and P2G systems is established to realize the low-carbon economic operation of P2G systems. On the energy storage side, the concept of "state of carbon" is introduced to describe the carbon emission characteristics of the ESS to exploit the potential of coordinated low-carbon dispatch in terms of both energy production and storage. In addition, a low-carbon economic dispatch model that considers multiple uncertainties, including wind power output, electricity price, and load demands, is established. To solve the model efficiently, a parallel multidimensional approximate dynamic programming algorithm is adopted, while the solution efficiency is significantly improved over that of stochastic optimization without losing solution accuracy under a multilayer parallel loop nesting framework. The low-carbon economic dispatch method of IESs is composed of the extended carbon emission flow model, low-carbon economic dispatch model, and the parallel multidimensional approximate dynamic programming algorithm. The effectiveness of the proposed method is verified on E14-H6-G6 and E57-H12-G12 systems.**

Index Terms—**Low-carbon economic dispatch, carbon emission flow, state of carbon, parallel multidimensional approximate dynamic programming, integrated energy system (IES).**

Manuscript received: October 11, 2023; revised: January 5, 2024; accepted: May 8, 2024. Date of CrossCheck: May 8, 2024. Date of online publication: May 21, 2024.

This work was supported by the Chinese Postdoctoral Science Foundation (No. 2023M734092), National Natural Science Foundation of China (No. 52107111), and Shandong Provincial Natural Science Foundation of China (No. ZR2022ME219).

Y. Zhang, P. Sun, X. Ji (corresponding author), and P. Ye are with Shandong University of Science and Technology, Qingdao 266590, China (e-mail: ymzhang2019@sdust.edu.cn; pksun@sdust.edu.cn; xqji@sdust.edu.cn; ypf@sdust.edu.cn).

F. Wen is with the Hainan Institute, Zhejiang University, Sanya 572000, China, and he is also with the School of Electrical Engineering, Zhejiang University, Hangzhou 310027, China (e-mail: fushuan.wen@gmail.com).

M. Yang is with the Key Laboratory of Power System Intelligent Dispatch and Control, Shandong University, Jinan 250061, China (e-mail: myang@sdu.edu.cn).

DOI: 10.35833/MPCE.2023.000743

I. Introduction

THE clean and low-carbon transformation of energy systems has been the primary focus in efforts to curb global greenhouse gas emissions [1], [2]. However, the volatility and uncertainty of intermittent renewable energy-based generation outputs have brought new challenges to the low-carbon operation of energy systems [3], [4]. In an integrated energy system (IES), the coupling properties and mutual conversion capabilities of electricity, heat energy, and natural gas provide effective means to mitigate the intermittency of renewable energy-based generation. Therefore, fully exploiting the low-carbon potential of IESs in production, transmission, conversion, distribution, and storage is critical in coping with uncertain power outputs from intermittent renewable energy-based generation units and in achieving low-carbon dispatch [5], [6].

Studies have been conducted on the optimal operation of IESs [7]-[10]. In addition, [11] proposed a distributionally robust optimal dispatching model for an electricity-heat IES under the condition of wind power uncertainties and demonstrated that coordination between the electric and heat subsystems could effectively increase wind power accommodation. Reference [12] proposed a two-stage optimization method for a community-integrated energy system and verified that the coupled operation of electricity-gas-heat subsystems could improve the operational economics of the IES. As an effective means of accommodating intermittent renewable energy-based generation, power-to-gas (P2G) system is gradually being applied in the energy industry [13], [14]. P2G systems convert electricity into hydrogen, which can then be stored, transported, and converted into other forms of energy. Reference [15] established a day-ahead IES dispatching model considering P2G systems to minimize IES operational costs and verified that the P2G systems could effectively increase wind power accommodation. However, the aforementioned studies were essentially focused on electricity with the goal of minimizing IES operational costs while ignoring additional costs derived from carbon emission. And the dispatch modes, in which electricity and carbon are separated from each other, restrict the low-carbon and economic operation of the IES.

To achieve low-carbon and economic operations of IESs, numerous studies have been conducted on optimal dispatching of IES in terms of carbon [16]-[18]. In [19], a carbon tax mechanism was incorporated into the economic dispatch model of IES to reduce the carbon emission of coal-fired units. Carbon capture and storage (CCS) system is an effective emission reduction technology that has received widespread attention [20], [21]. In [22], a low-carbon economic dispatch problem was investigated for intermittent renewable energy-based generation and coal-fired units with CCS systems. However, in terms of an electricity-gas-heat-coupled IES, a quantitative analysis of the energy savings and emission reduction benefits from CCS system has rarely been reported.

A thorough analysis of the carbon emission flow (CEF) process can also greatly assist in evaluating the effects of low-carbon dispatch. CEF theory was developed in an earlier study and provided a new analytical tool for low-carbon dispatch. In [23] and [24], CEF models were proposed that can trace the embedded CO_2 emissions of energy usage. However, in these studies, energy storage systems (ESSs) were not incorporated into the CEF model, which affected the rationality of the carbon emission results. The traditional CEF model is known to have difficulty in accurately depicting the carbon emission characteristics of an ESS-based system because of the variety and time coupling of ESS states. Therefore, extending the CEF model for better application to the low-carbon dispatch of IES is necessary.

To solve these problems, an extended CEF (ECEF) model is introduced, and a CCS-P2G-ESS-coordinated low-carbon dispatch model is proposed. The major contributions of this study are as follows.

1) A CCS-P2G synergistic operation mode is proposed to form an integrated generation-capture-utilization framework of carbon emission, which reduces the cost of purchasing CO_2 and improves the operating economics of the IES.

2) Based on the effects of the charging and discharging states of the ESS on the CEF of the system, as well as the dynamic relationship between the carbon emission of the ESS and the energy in the entire dispatching cycle, the concept of "state of carbon" (SOCB) is proposed to express the carbon emission characteristics of the ESS.

3) The SOCB is combined with the traditional CEF model to generate the proposed ECEF model, which considers ESS and thus effectively describes the CEF path in the entire process of the IES dispatch period. The ECEF model also provides a new assessment criterion for the rationality and effectiveness of a low-carbon dispatch strategy of IES.

II. Synergistic Operation of CCS and P2G Systems

A. IES Architecture

The high carbon emission of conventional coal-fired units makes it difficult for IESs to operate at low-carbon levels. In this study, CCS and P2G systems are coupled to form a CCS-P2G synergistic operation mode, which can provide sufficient CO_2 feedstock for P2G systems. The architecture of IES with a CCS-P2G synergistic operation mode is shown in Supplemental Material A Fig. SA1.

The IES consists of conventional coal-fired units, coal-fired units with CCS system, ESS devices, wind turbines, and electrical loads. The heat system (HS) contains heat storage tanks (HSTs) and heat loads. Energy-coupling devices include P2G systems, combined heat and power (CHP) systems, and gas turbines. A portion of the electricity in the system is converted to natural gas through P2G systems, and a portion of the natural gas energy is converted to electricity and heat energy through the CHP system.

B. CCS-P2G Synergistic Operation Mode

CCS-P2G synergistic operation mode is shown in Supplemental Material A Fig. SA2. The P2G systems convert electricity to natural gas through water electrolysis and methanation. The P2G systems use surplus wind power, solar power, and other renewable energy-based generation to electrolyze water to produce H_2 and O_2. The CO_2 captured from the coal-fired units and the H_2 produced in the electrolysis of water are then combined to produce CH_4 through the methanation process. The CCS-P2G synergistic operation mode reduces the carbon emission of traditional coal-fired units while using CO_2 in the system. This reduces the cost of purchasing CO_2 for the P2G systems.

III. ECEF Model Considering Energy Storage

Based on CEF theory, we assume that a virtual "carbon flow" runs along with the branch power flow, and the CO_2 generated at the source side is transferred to the load side by branches (i.e., lines and transformers). The "carbon flow" intuitively indicates the flow direction of carbon emission during system operation, thereby providing a perspective for low-carbon dispatch of the IES.

A. CEF Model

In this study, the key elements of the CEF model are based on the theories presented in [25] and [26].

1) CEF Rate (CEFR)

In this study, the CEFR is used to characterize the carbon emission per unit time through branches or nodes:

$$F^{\mathrm{cefr}}=\frac{\mathrm{d}F^{\mathrm{cef}}}{\mathrm{d}t} \tag{1}$$

where F^{cefr} is the CEFR; F^{cef} is the CEF through the branches or nodes; and t is the scheduling time.

2) Carbon Intensity (CI)

CI is used to characterize carbon emission per unit of energy. CI is typically classified into generation CI (GCI), branch CI (BCI), port CI (PCI), and node CI (NCI). GCI is related to the power (or carbon emission per unit of energy) at the source side. BCI is the CI of the energy flowing along a branch, and PCI is the CI associated with the input or output energy of an energy-coupling device. NCI represents the superposition effect of CI. In other words, the CI of each branch connected to the same node should be aggregated. NCI is the average carbon emission per unit of energy injected into the node and is equal to the ratio of the total CI to the total energy injected into the node:

$$NCI_{i,t}=\frac{\sum\limits_{b^{\mathrm{e}}\in\Omega_i^{\mathrm{e+}}}P_{b^{\mathrm{e}},t}^{\mathrm{branch}}\cdot BCI_{b^{\mathrm{e}},t}+\sum\limits_{g\in\Omega_i^{\mathrm{G}}}P_{g,t}^{\mathrm{coal\_fired\_unit}}\cdot GCI_{g,t}}{\sum\limits_{b^{\mathrm{e}}\in\Omega_i^{\mathrm{e+}}}P_{b^{\mathrm{e}},t}^{\mathrm{branch}}+\sum\limits_{g\in\Omega_i^{\mathrm{G}}}P_{g,t}^{\mathrm{coal\_fired\_unit}}}\quad \forall i\in I,\forall t\in T \tag{2}$$

where $NCI_{i,t}$ is the carbon emission intensity of node i at time t; $P_{b^e,t}^{\text{branch}}$ is the power flowing through branch b^e at time t; $BCI_{b^e,t}$ is the carbon emission intensity of branch b^e at time t; $P_{g,t}^{\text{coal\_fired\_unit}}$ is the power output of coal-fired unit g at time t; $GCI_{g,t}$ is the carbon emission intensity of coal-fired unit g at time t; Ω_i^{e+} is the set of branches that inject power into node i; Ω_i^{G} is the set of coal-fired units that inject power into node i; I is the set of all nodes; and T is the set of periods.

Figure 1 shows a simple power system to illustrate the relationship between CEF and electricity flow, where $P_{G1,t}^{\text{coal\_fired\_unit}}$, $P_{G2,t}^{\text{coal\_fired\_unit}}$, and $P_{G3,t}^{\text{coal\_fired\_unit}}$ are the power outputs of coal-fired units G1, G2, and G3 at time t, respectively; $P_{(i,j),t}^{\text{branch}}$ is the power flow from node i to node j at time t; $GCI_{G1,t}$, $GCI_{G2,t}$, and $GCI_{G3,t}$ are the GCIs of coal-fired units G1, G2, and G3 at time t, respectively; and $BCI_{(i,j),t}$ is the BCI of branch from node i to node j at time t. NCI of node 2 at time t can be expressed as:

$$NCI_{2,t}=\frac{P_{(1,2),t}^{\text{branch}}\cdot BCI_{(1,2),t}+P_{G2,t}^{\text{coal\_fired\_unit}}\cdot GCI_{G2,t}}{P_{(1,2),t}^{\text{branch}}+P_{G2,t}^{\text{coal\_fired\_unit}}}\quad \forall t\in T \tag{3}$$

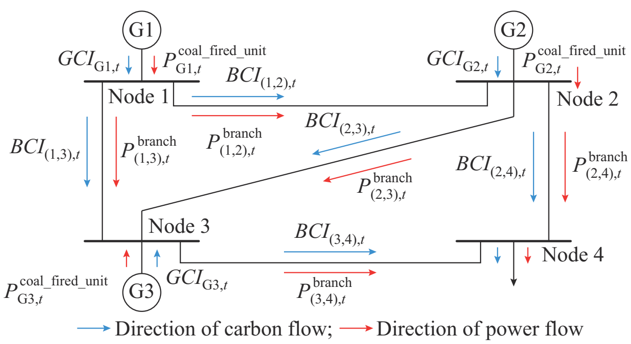

Fig. 1. Relationship between CEF and electricity flow.

The BCI of a branch is determined by the NCI of the sending node of that branch. Therefore, the BCI of branch from node 1 to node 2 at time t can be expressed as:

$$BCI_{(1,2),t}=NCI_{1,t}\quad \forall t\in T \tag{4}$$

We can then rewrite (3) as:

$$NCI_{2,t}=\frac{P_{(1,2),t}^{\text{branch}}\cdot NCI_{1,t}+P_{G2,t}^{\text{coal\_fired\_unit}}\cdot GCI_{G2,t}}{P_{(1,2),t}^{\text{branch}}+P_{G2,t}^{\text{coal\_fired\_unit}}}\quad \forall t\in T \tag{5}$$

The carbon emission of node i at time t can be calculated by:

$$M_{i,t}=NCI_{i,t}\cdot D_{i,t}\Delta t\quad \forall i\in I, \forall t\in T \tag{6}$$

where $M_{i,t}$ is the carbon emission of node i at time t; $D_{i,t}$ is the load power of node i at time t; and Δt is the unit scheduling period, which is set to be one hour in this study.

Thus far, a CEF model in an electric network has been established, and the relationship between "carbon flow" and "power flow" has been clarified, thereby endowing the virtual CEF process with a clear physical meaning. In addition, the distribution of CEF in the entire network can be deduced based solely on the GCI and the power flowing into the node, which is simple and practical.

Similarly, the CEFs in the heat and natural gas networks accompany the energy flow of fluids in the heat and natural gas pipelines, which is modeled in a similar manner as that of the electricity network and is therefore not detailed in this study [23].

B. CEF Model of Energy-coupling Devices

In the process of converting energy-coupling devices into different types of energy, carbon emission is transferred to different energy systems. The carbon emission transfer characteristics in the energy conversion process can be analyzed using the CEF model of the energy-coupling device. This study uses the method proposed in [27] to classify energy-coupling devices into single-input-single-output (SISO) devices such as gas turbines and P2G systems, and single-input-multi-output (SIMO) devices such as CHPs. Their carbon-emission flow models are established separately.

1) SISO Energy-coupling Devices

According to the principle of carbon conservation, the carbon emission associated with the input energy of SISO devices are allocated to the output energy. In other words, the total CEFR at the input port is equal to that at the output port, and can be expressed as:

$$PCI_{eq,t}^{\text{in}}\cdot P_{eq,t}^{\text{in}}=PCI_{eq,t}^{\text{out}}\cdot P_{eq,t}^{\text{out}} \tag{7}$$

where $PCI_{eq,t}^{\text{in}}$ is the input PCI of the energy-coupling device eq at time t; $P_{eq,t}^{\text{in}}$ is the input power of energy-coupling device eq at time t; $PCI_{eq,t}^{\text{out}}$ is the output PCI of the energy-coupling device eq at time t; and $P_{eq,t}^{\text{out}}$ is the output power of energy-coupling device eq at time t.

If the conversion efficiency of the SISO energy-coupling device eq is η_{eq}, the relationship between the input and output of energy can be expressed as:

$$P_{eq,t}^{\text{out}}=\eta_{eq}P_{eq,t}^{\text{in}} \tag{8}$$

where η_{eq} is the conversion efficiency of the SISO energy-coupling device eq.

Thus, (7) can be rewritten as:

$$PCI_{eq,t}^{\text{out}}=\frac{PCI_{eq,t}^{\text{in}}}{\eta_{eq}} \tag{9}$$

Based on the CEF model described by (9), we can change the perspective from energy to carbon emission to analyze the relationship between the input and output of the SISO device.

2) SIMO Energy-coupling Devices

The principle of carbon conservation still holds for SIMO energy-coupling devices, and all carbon emission associated with input energy must be allocated to the output ports. In terms of energy conversion, for a typical backpressure CHP system, the output electric and heat energy levels are proportional to the input natural gas energy, and can be expressed as:

$$\begin{cases} P_{c,t}^{\text{CHP}}=G_{c,t}^{\text{CHP}}\eta_c^{\text{e}} \\ H_{c,t}^{\text{CHP}}=G_{c,t}^{\text{CHP}}\eta_c^{\text{h}} \end{cases} \tag{10}$$

where $P_{c,t}^{\text{CHP}}$ is the electric power of CHP system c at time t; $G_{c,t}^{\text{CHP}}$ is the natural gas flow rate of CHP system c at time t; η_c^{e} is the gas-electricity conversion efficiency of CHP system c; $H_{c,t}^{\text{CHP}}$ is the heat power of CHP system c at time t; and η_c^{h}

is the gas-heat conversion efficiency of CHP system c.

In terms of carbon emission, the total CEFR of the input port is equal to that of the output ports, and the PCI of the input and output ports can be expressed as:

$$PCI_{c,t}^{\text{e, out}} \cdot P_{c,t}^{\text{CHP}} + PCI_{c,t}^{\text{h, out}} \cdot H_{c,t}^{\text{CHP}} = PCI_{c,t}^{\text{in}} \cdot G_{c,t}^{\text{CHP}} \tag{11}$$

where $PCI_{c,t}^{\text{e, out}}$ is the PCI of the electric output port of CHP system c at time t; $PCI_{c,t}^{\text{h, out}}$ is the PCI of the heat output port of CHP system c at time t; and $PCI_{c,t}^{\text{in}}$ is the input port PCI of CHP system c at time t.

The PCI of the electricity and heat energy output ports are assumed to be inversely proportional to the conversion efficiency:

$$\frac{PCI_{c,t}^{\text{e, out}}}{\eta_c^{\text{h}}} = \frac{PCI_{c,t}^{\text{h, out}}}{\eta_c^{\text{e}}} \tag{12}$$

Substituting (12) into (11) yields:

$$\begin{cases} PCI_{c,t}^{\text{e, out}} = \dfrac{PCI_{c,t}^{\text{in}}}{2\eta_c^{\text{e}}} \\ PCI_{c,t}^{\text{h, out}} = \dfrac{PCI_{c,t}^{\text{in}}}{2\eta_c^{\text{h}}} \end{cases} \tag{13}$$

Equation (13) is thus the CEF model of the SIMO energy-coupling device.

C. CEF Model of Energy Storage Devices

Devices in an IES can be divided into three categories according to the methods of energy utilization: energy-discharging devices such as generators, energy-consumption devices such as various types of loads, and energy-coupling devices such as P2G systems. An ESS has two states: energy-discharging state and energy-consumption state. An ESS in an energy-consumption state is equivalent to a special load that can absorb some of the carbon emission. However, in an energy-discharging state, it is equivalent to a special power-generation device that releases some of the carbon emission. The diversity of ESS states increases the complexity of the associated CEF models. Therefore, the concept of SOCB for ESSs is proposed and is used to characterize the relationship between the energy and absorbed carbon emission in ESSs.

When the ESS is charging, carbon emission flows into the ESS along with electric energy, as expressed by:

$$M_{e,t}^{\text{cha}} = P_{e,t}^{\text{cha}} \cdot NCI_{e,t}^{\text{ESS}} \cdot \Delta t \tag{14}$$

where $M_{e,t}^{\text{cha}}$ is the carbon emission flowing into ESS e at time t; $P_{e,t}^{\text{cha}}$ is the charging power of ESS e at time t; and $NCI_{e,t}^{\text{ESS}}$ is the NCI of the node where ESS e is located at time t.

When the ESS is discharging, carbon emission is released from the ESS along with electrical energy, as expressed by:

$$M_{e,t}^{\text{dis}} = P_{e,t}^{\text{dis}} \cdot GCI_{e,t}^{\text{ESS}} \cdot \Delta t = \frac{P_{e,t}^{\text{dis}}}{\eta_e^{\text{dis}}} \cdot SOCB_{e,t-1} \cdot \Delta t \tag{15}$$

where $M_{e,t}^{\text{dis}}$ is the carbon emission released by ESS e at time t; $P_{e,t}^{\text{dis}}$ is the discharging power of ESS e at time t; $GCI_{e,t}^{\text{ESS}}$ is the GCI of ESS e at time t; η_e^{dis} is the discharging efficiency of ESS e; and $SOCB_{e,t}$ is the SOCB of ESS e at time t.

The SOCB of the ESS is defined as:

$$SOCB_{e,t} = \frac{SOCB_{e,t-1} E_{e,t-1} + M_{e,t}^{\text{cha}} - M_{e,t}^{\text{dis}}}{E_{e,t}} \tag{16}$$

where $E_{e,t}$ is the available capacity of ESS e at time t.

In summary, a unified CEF model for each component of the IES is established by mapping the energy storage/release process to the carbon emission storage/release process. Thus, the application scope of the CEF model is extended.

IV. Low-carbon Economic Dispatch Model of IES

This study establishes a low-carbon economic dispatch model of IES and employs a parallel multi-dimensional approximate dynamic programming (PMADP) algorithm for its solution. The solution methodology and process of the PMADP are shown in Supplemental Material B (B1)-(B6), algorithms 1 and 2.

A. Objective Function

The objective of low-carbon economic dispatch in an IES is to minimize the operating and carbon emission costs while considering the operational constraints of the power system, heat system (HS), and natural gas system (NGS). In this study, the operating costs of the CHP system and gas turbines are integrated into the purchasing cost of NGS:

$$F = E\{F_n\} \quad n \in N \tag{17}$$

$$F_n = \min\left\{\sum_{t \in T} (f_{n,t}^{\text{e}} + f_{n,t}^{\text{h}} + f_{n,t}^{\text{g}}) + f_n^{\text{c}}\right\} \quad n \in N \tag{18}$$

where F is the objective function; $E\{F_n\}$ is the expected value of F_n; F_n is the total operating cost of the IES in scenario n; $f_{n,t}^{\text{e}}$ is the operating cost of the power system at time t in scenario n; $f_{n,t}^{\text{h}}$ is the operating cost of the HS at time t in scenario n; $f_{n,t}^{\text{g}}$ is the operating cost of the NGS at time t in scenario n; f_n^{c} is the carbon emission costs during the scheduling horizon; and N is the set of scenarios.

1) Carbon Emission Cost

The carbon emission cost f_n^{c} is usually calculated daily, which includes the CO_2 transportation and storage cost $f_n^{\text{c, trans}}$, carbon quota overage cost $f_n^{\text{c, cost}}$, and CO_2 purchasing cost of P2G systems $f_n^{\text{c, buy}}$. This can be formulated as in [28].

$$f_n^{\text{c}} = f_n^{\text{c, trans}} + f_n^{\text{c, cost}} + f_n^{\text{c, buy}} \tag{19}$$

$$\begin{cases} f_n^{\text{c, trans}} = C^{\text{c, trans}} \left(\sum\limits_{t \in T} \sum\limits_{k \in K} M_{k,n,t}^{\text{CCS}} - \sum\limits_{t \in T} \sum\limits_{u \in U} M_{u,n,t}^{\text{P2G}} \right) \\ f_n^{\text{c, cost}} = C^{\text{c, deal}} \Bigg[M_{n,t}^{\text{all}} - \sum\limits_{t \in T} \sum\limits_{g \in G} \lambda_g^{\text{coal\_fired\_unit}} P_{g,n,t}^{\text{coal\_fired\_unit}} - \\ \quad \sum\limits_{t \in T} \sum\limits_{k \in K} \lambda_k^{\text{CCS}} P_{k,n,t}^{\text{CCS}} - \sum\limits_{t \in T} \sum\limits_{c \in C} \lambda_c^{\text{CHP}} (P_{c,n,t}^{\text{CHP}} + H_{c,n,t}^{\text{CHP}}) - \\ \quad \sum\limits_{t \in T} \sum\limits_{r \in R} \lambda_r^{\text{gas\_turbine}} P_{r,n,t}^{\text{gas\_turbine}} - \sum\limits_{t \in T} \sum\limits_{o \in O} \lambda_o^{\text{external\_grid}} P_{o,n,t}^{\text{external\_grid}} \Bigg] \\ f_n^{\text{c, buy}} = C^{\text{buy, CO}_2} \left(\sum\limits_{t \in T} \sum\limits_{u \in U} \tau_u^{\text{P2G}} P_{u,n,t}^{\text{P2G}} - \sum\limits_{t \in T} \sum\limits_{k \in K} M_{k,n,t}^{\text{CCS}} \right) \end{cases} \tag{20}$$

where $C^{\text{c, trans}}$ is the cost coefficient for CO_2 transportation and storage; $M_{k,n,t}^{\text{CCS}}$ is the CO_2 captured by the CCS system from coal-fired unit k at time t in scenario n; $M_{u,n,t}^{\mathrm{P2G}}$ is the CO_2 consumed by P2G system u at time t in scenario n; $C^{\mathrm{c,deal}}$ is the cost coefficient for CO_2 transaction; $M_{n,t}^{\mathrm{all}}$ is the total carbon emission of the IES at time t in scenario n; $\lambda_g^{\mathrm{coal\_fired\_unit}}$ is the carbon emission allowance factor for coal-fired unit g; $P_{g,n,t}^{\mathrm{coal\_fired\_unit}}$ is the power output of coal-fired unit g at time t in scenario n; λ_k^{CCS} is the carbon emission allowance factor for coal-fired unit k with CCS system; $P_{k,n,t}^{\mathrm{CCS}}$ is the power output of coal-fired unit k with CCS system at time t in scenario n; λ_c^{CHP} is the carbon emission allowance factor for CHP system c; $P_{c,n,t}^{\mathrm{CHP}}$ is the electric power of CHP system c at time t in scenario n; $H_{c,n,t}^{\mathrm{CHP}}$ is the heat power of CHP system c at time t in scenario n; $\lambda_r^{\mathrm{gas\_turbine}}$ is the carbon emission allowance factor for gas turbine r; $P_{r,n,t}^{\mathrm{gas\_turbine}}$ is the power output of gas turbine r at time t in scenario n; $\lambda_o^{\mathrm{external\_grid}}$ is the carbon emission allowance factor for the external grid o; $P_{o,n,t}^{\mathrm{external\_grid}}$ is the power purchased from the external grid o at time t in scenario n; $C^{\mathrm{buy,CO_2}}$ is the cost coefficient for CO_2 purchasing; τ_u^{P2G} is the conversion efficiency of P2G system u; $P_{u,n,t}^{\mathrm{P2G}}$ is the energy consumption of P2G system u at time t in scenario n; K is the set of coal-fired units containing CCS systems; U is the set of P2G systems; G is the set of coal-fired units; C is the set of CHP systems; R is the set of gas turbines; and O is the set of external grids.

2) Power System Operating Cost

The power system operating cost is expressed as:

$$f_{n,t}^{\mathrm{e}}=\sum_{g\in G}C_g^{\mathrm{coal\_fired\_unit}}P_{g,n,t}^{\mathrm{coal\_fired\_unit}}+\sum_{r\in R}C_r^{\mathrm{gas\_turbine}}P_{r,n,t}^{\mathrm{gas\_turbine}}+\sum_{o\in O}p_{n,t}^{\mathrm{external\_grid}}P_{o,n,t}^{\mathrm{external\_grid}}+\sum_{i\in I}C^{\mathrm{np}}P_{i,n,t}^{\mathrm{np}}+\sum_{e\in E}C_e^{\mathrm{cha}}P_{e,n,t}^{\mathrm{cha}}+\sum_{e\in E}C_e^{\mathrm{dis}}P_{e,n,t}^{\mathrm{dis}}+\sum_{w\in W}C^{\mathrm{nw}}P_{w,n,t}^{\mathrm{nw}}\quad \forall n\in N,\forall t\in T \tag{21}$$

$$P_{w,n,t}^{\mathrm{nw}}=\max(P_{w,n,t}^{\mathrm{f}}-P_{w,n,t}^{\mathrm{wind}},0)\quad \forall n\in N,\forall t\in T \tag{22}$$

where $C_g^{\mathrm{coal\_fired\_unit}}$ is the operating cost coefficient of coal-fired unit g; $C_r^{\mathrm{gas\_turbine}}$ is the operating cost coefficient of gas turbine r; $p_{n,t}^{\mathrm{external\_grid}}$ is the electricity price at time t in scenario n; C^{np} is the penalty factor of load shedding; $P_{i,n,t}^{\mathrm{np}}$ is the shed load power at node i at time t in scenario n; C_e^{cha} is the charging cost coefficient of ESS e; $P_{e,n,t}^{\mathrm{cha}}$ is the charging power of ESS e at time t in scenario n; C_e^{dis} is the discharging cost coefficient of ESS e; $P_{e,n,t}^{\mathrm{dis}}$ is the discharging power of ESS e at time t in scenario n; C^{nw} is the penalty factor of wind curtailment; $P_{w,n,t}^{\mathrm{nw}}$ is the curtailed wind power of wind turbine w at time t in scenario n; $P_{w,n,t}^{\mathrm{f}}$ is the predicted power of wind turbine w at time t in scenario n; $P_{w,n,t}^{\mathrm{wind}}$ is the accommodated power of wind turbine w at time t in scenario n; E is the set of ESSs; and W is the set of wind turbines.

3) HS Operating Cost

The HS operating cost is expressed as:

$$f_{n,t}^{\mathrm{h}}=\sum_{z\in Z}C^{\mathrm{nsh}}H_{z,n,t}^{\mathrm{nsh}}\quad \forall n\in N,\forall t\in T \tag{23}$$

where C^{nsh} is the penalty factor for heat load shedding; $H_{z,n,t}^{\mathrm{nsh}}$ is the shed heat load at node z at time t in scenario n; and Z is the set of nodes in the heat network.

4) NGS Operating Cost

The NGS operating cost is expressed as:

$$f_{n,t}^{\mathrm{g}}=\sum_{s\in S}C_s^{\mathrm{source}}G_{s,n,t}^{\mathrm{source}}+\sum_{a\in A}C^{\mathrm{nsg}}G_{a,n,t}^{\mathrm{nsg}}\quad \forall n\in N,\forall t\in T \tag{24}$$

where C_s^{source} is the natural gas cost from source s; $G_{s,n,t}^{\mathrm{source}}$ is the amount of natural gas output from source s at time t in scenario n; C^{nsg} is the penalty factor for natural gas load shedding; $G_{a,n,t}^{\mathrm{nsg}}$ is the shed gas load at node a at time t in scenario n; S is the set of gas sources; and A is the set of gas network nodes.

B. Constraints

The constraints in the low-carbon economic dispatch model of IES include the power system, HS, and NGS operational constraints as well as energy-coupling device constraints.

1) Power System Operational Constraints

The power system mainly includes the power balance constraint, operational constraints of coal-fired units with CCS system, branch power flow constraints, unit start-up and shut-down constraints, and ramping constraints.

$$\sum_{g\in\Omega_i^{\mathrm{G}}}P_{g,n,t}^{\mathrm{coal\_fired\_unit}}+\sum_{k\in\Omega_i^{\mathrm{K}}}P_{k,n,t}^{\mathrm{net}}+\sum_{c\in\Omega_i^{\mathrm{C}}}P_{c,n,t}^{\mathrm{CHP}}+\sum_{r\in\Omega_i^{\mathrm{R}}}P_{r,n,t}^{\mathrm{gas\_turbine}}+\sum_{w\in\Omega_i^{\mathrm{W}}}P_{w,n,t}^{\mathrm{wind}}+\sum_{o\in\Omega_i^{\mathrm{O}}}P_{o,n,t}^{\mathrm{external\_grid}}+\sum_{e\in\Omega_i^{\mathrm{E}}}P_{e,n,t}^{\mathrm{dis}}-\sum_{e\in\Omega_i^{\mathrm{E}}}P_{e,n,t}^{\mathrm{cha}}-\sum_{q\in\Omega_i^{Q}}P_{q,n,t}^{\mathrm{pump}}-\sum_{u\in\Omega_i^{\mathrm{U}}}P_{u,n,t}^{\mathrm{P2G}}+\sum_{b^{\mathrm{e}}\in\Omega_i^{\mathrm{e}+}}P_{b^{\mathrm{e}},n,t}^{\mathrm{branch}}-\sum_{b^{\mathrm{e}}\in\Omega_i^{\mathrm{e}-}}P_{b^{\mathrm{e}},n,t}^{\mathrm{branch}}=D_{i,n,t}-P_{i,n,t}^{\mathrm{np}}\quad \forall n\in N,\forall t\in T \tag{25}$$

where Ω_i^{K} is the set of coal-fired units with CCS systems that injects power to node i; $P_{k,n,t}^{\mathrm{net}}$ is the net output power of coal-fired unit k with CCS system at time t in scenario n; Ω_i^{C} is the set of CHP systems that injects power to node i; Ω_i^{R} is the set of gas turbines that injects power to node i; Ω_i^{W} is the set of wind turbines that injects power to node i; Ω_i^{O} is the set of external grids connected to node i; Ω_i^{E} is the set of ESSs that is connected to node i; Ω_i^{Q} is the set of pumps that is connected to node i; $P_{q,n,t}^{\mathrm{pump}}$ is the power consumption of water pump q at time t in scenario n; Ω_i^{U} is the set of P2G systems that injects power to node i; $\Omega_i^{\mathrm{e}+}$ is the set of outflow branches of node i; $\Omega_i^{\mathrm{e}-}$ is the set of inflow branches of node i; $P_{b^{\mathrm{e}},n,t}^{\mathrm{branch}}$ is the power flowing through branch b^{e} at time t in scenario n; and $D_{i,n,t}$ is the predicted electrical load at node i at time t in scenario n.

Operational constraints of coal-fired units with CCS system are expressed as:

$$\begin{cases}P_{k,n,t}^{\mathrm{CCS}}=P_{k,n,t}^{\mathrm{net}}+P_{k,n,t}^{\mathrm{std}}+P_{k,n,t}^{\mathrm{opt}}\\ P_{k,n,t}^{\mathrm{opt}}=\chi_k^{\mathrm{opt}}M_{k,n,t}^{\mathrm{CCS}}\\ M_{k,n,t}^{\mathrm{CCS}}=\theta_k^{\mathrm{opt}}M_{k,n,t}\\ 0\le\theta_k^{\mathrm{opt}}\le\theta_k^{\mathrm{CCS\_max}}\end{cases}\quad \forall k\in K,\forall t\in T,\forall n\in N \tag{26}$$

where $P_{k,n,t}^{\mathrm{std}}$ is the fixed power consumption of coal-fired unit k with CCS system at time t in scenario n; $P_{k,n,t}^{\mathrm{opt}}$ is the operational power consumption of coal-fired unit k with CCS system at time t in scenario n [29]; χ_k^{opt} is the energy consumption of the CCS system to capture per unit CO_2; θ_k^{opt} is the carbon-capture efficiency of coal-fired unit k with CCS system; $M_{k,n,t}$ is the total carbon emission of coal-fired unit k with CCS system at time t in scenario n; and $\theta_k^{\mathrm{CCS\_max}}$ is the upper limit of carbon-capture efficiency of coal-fired unit k with CCS system.

The branch power flow constraints are expressed as:

$$\begin{cases} P^{\text{branch}}_{b^{\text{e}},n,t} = \dfrac{\theta_{i,n,t} - \theta_{j,n,t}}{x_{b^{\text{e}}}} \\ P^{\text{branch}}_{b^{\text{e}},n,t} \le P^{\max}_{b^{\text{e}}} \\ \theta^{\min}_i \le \theta_{i,n,t} \le \theta^{\max}_i \\ \theta^{\min}_j \le \theta_{j,n,t} \le \theta^{\max}_j \end{cases} \quad \forall i \in \Omega^{\text{e}+}_{b^{\text{e}}}, \forall j \in \Omega^{\text{e}-}_{b^{\text{e}}}, \forall n \in N, \forall t \in T \tag{27}$$

where $\theta_{i,n,t}$ is the phase angle of node i that is the first node of branch b^{e} at time t in scenario n; $\theta_{j,n,t}$ is the phase angle of node j that is the end node of branch b^{e} at time t in scenario n; $x_{b^{\text{e}}}$ is the reactance of branch b^{e}; $P^{\max}_{b^{\text{e}}}$ is the upper power limit of branch b^{e}; $\theta^{\min}_i$ and $\theta^{\max}_i$ are the lower and upper phase angle limits of node i that is the first node of branch b^{e}, respectively; $\theta^{\min}_j$ and $\theta^{\max}_j$ are the lower and upper phase angle limits of node j that is the end node of branch b^{e}, respectively; $\Omega^{\text{e}+}_{b^{\text{e}}}$ is the set of first nodes of branch b^{e}; and $\Omega^{\text{e}-}_{b^{\text{e}}}$ is the set of end nodes of branch b^{e}.

The unit operating limits and ramping constraints are expressed as:

$$\begin{cases} P^{\text{coal\_fired\_unit, min}}_g \le P^{\text{coal\_fired\_unit}}_{g,n,t} \le P^{\text{coal\_fired\_unit, max}}_g \\ P^{\text{net, min}}_k \le P^{\text{net}}_{k,n,t} \le P^{\text{net, max}}_k \\ P^{\text{gas\_turbine, min}}_r \le P^{\text{gas\_turbine}}_{r,n,t} \le P^{\text{gas\_turbine, max}}_r \\ P^{\text{CHP, min}}_c \le P^{\text{CHP}}_{c,n,t} \le P^{\text{CHP, max}}_c \end{cases}$$
$$\forall g \in G, \forall k \in K, \forall r \in R, \forall c \in C, \forall n \in N, \forall t \in T \tag{28}$$

$$\begin{cases} P^{\text{coal\_fired\_unit}}_{g,n,t} - P^{\text{coal\_fired\_unit}}_{g,n,t-\Delta t} \le r^{\text{coal\_fired\_unit, up}}_g \\ P^{\text{net}}_{k,n,t} - P^{\text{net}}_{k,n,t-\Delta t} \le r^{\text{net, up}}_k \\ P^{\text{gas\_turbine}}_{r,n,t} - P^{\text{gas\_turbine}}_{r,n,t-\Delta t} \le r^{\text{gas\_turbine, up}}_r \\ P^{\text{CHP}}_{c,n,t} - P^{\text{CHP}}_{c,n,t-\Delta t} \le r^{\text{CHP, up}}_c \end{cases}$$
$$\forall g \in G, \forall k \in K, \forall r \in R, \forall c \in C, \forall n \in N, \forall t \in T \tag{29}$$

$$\begin{cases} P^{\text{coal\_fired\_unit}}_{g,n,t-\Delta t} - P^{\text{coal\_fired\_unit}}_{g,n,t} \le r^{\text{coal\_fired\_unit, down}}_g \\ P^{\text{net}}_{k,n,t-\Delta t} - P^{\text{net}}_{k,n,t} \le r^{\text{net, down}}_k \\ P^{\text{gas\_turbine}}_{r,n,t-\Delta t} - P^{\text{gas\_turbine}}_{r,n,t} \le r^{\text{gas\_turbine, down}}_r \\ P^{\text{CHP}}_{c,n,t-\Delta t} - P^{\text{CHP}}_{c,n,t} \le r^{\text{CHP, down}}_c \end{cases}$$
$$\forall g \in G, \forall k \in K, \forall r \in R, \forall c \in C, \forall n \in N, \forall t \in T \tag{30}$$

where $P^{\text{coal\_fired\_unit, min}}_g$ is the lower output power limit of coal-fired unit g; $P^{\text{coal\_fired\_unit, max}}_g$ is the upper output power limit of coal-fired unit g; $P^{\text{net, min}}_k$ is the lower output power limit of coal-fired unit k with CCS system; $P^{\text{net, max}}_k$ is the upper output power limit of coal-fired unit k with CCS system; $P^{\text{gas\_turbine, min}}_r$ is the lower output power limit of gas turbine r; $P^{\text{gas\_turbine, max}}_r$ is the upper output power limit of gas turbine r; $P^{\text{CHP, min}}_c$ is the lower output power limit of CHP system c; $P^{\text{CHP, max}}_c$ is the upper output power limit of CHP system c; $r^{\text{coal\_fired\_unit, up}}_g$ is the ramp up rate of coal-fired unit g; $r^{\text{net, up}}_k$ is the ramp up rate of coal-fired unit k with CCS system; $r^{\text{gas\_turbine, up}}_r$ is the ramp up rate of gas turbine r; $r^{\text{CHP, up}}_c$ is the ramp up rate of CHP system c; $r^{\text{coal\_fired\_unit, down}}_g$ is the ramp down rate of coal-fired unit g; $r^{\text{net, down}}_k$ is the ramp down rate of coal-fired unit k with CCS system; $r^{\text{gas\_turbine, down}}_r$ is the ramp down rate of gas turbine r; and $r^{\text{CHP, down}}_c$ is the ramp down rate of CHP system c.

The operating constraints of ESSs are expressed as:

$$\begin{cases} u^{\text{cha}}_{e,n,t} + u^{\text{dis}}_{e,n,t} \le 1 \\ u^{\text{cha}}_{e,n,t}, u^{\text{dis}}_{e,n,t} \in \{0,1\} \\ 0 \le P^{\text{cha}}_{e,n,t} \le u^{\text{cha}}_{e,n,t} P^{\text{cha, max}}_e \\ 0 \le P^{\text{dis}}_{e,n,t} \le u^{\text{dis}}_{e,n,t} P^{\text{dis, max}}_e \\ E_{e,n,t} = E_{e,n,t-\Delta t} + \eta^{\text{cha}}_e P^{\text{cha}}_{e,n,t} \Delta t - \\ \qquad \eta^{\text{dis}}_e P^{\text{dis}}_{e,n,t} \Delta t \\ E^{\min}_e \le E_{e,n,t} \le E^{\max}_e \\ E^{\text{end}}_{e,n} = E^{\text{init}}_{e,n} \end{cases} \quad \forall e \in E, \forall n \in N, \forall t \in T \tag{31}$$

where $u^{\text{cha}}_{e,n,t}$ is the binary variable representing the charging state of ESS e at time t in scenario n; $u^{\text{dis}}_{e,n,t}$ is the binary variable representing the discharging state of ESS e at time t in scenario n; $P^{\text{cha, max}}_e$ is the maximum charging power of ESS e; $P^{\text{dis, max}}_e$ is the maximum charging power of ESS e; η^{cha}_e is the charging efficiency of ESS e; $E_{e,n,t}$ is the available capacity of ESS e at time t in scenario n; $E^{\min}_e$ is the available minimum capacity of ESS e; $E^{\max}_e$ is the available maximum capacity of ESS e; $E^{\text{end}}_{e,n}$ is the available capacity of ESS e at the end of the dispatching cycle in scenario n; and $E^{\text{init}}_{e,n}$ is the available capacity of ESS e at the beginning of the dispatching cycle in scenario n.

2) HS Operational Constraints

As Fig. 2 shows, a typical HS consists of a heat station, pipelines, and a heat exchange station, where the heat station and heat exchange station act as the heat source and heat load, respectively. In scenario n, the HS constraints include the heat station operational constraints, heat network pipeline constraint, and heat exchange station operational constraint.

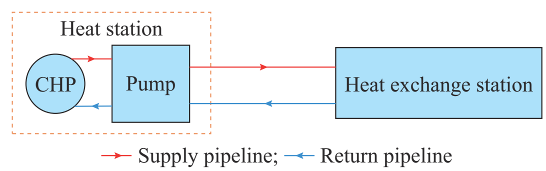

Fig. 2. Basic structure of HS.

1) Heat station constraints

The heat station constraints can be expressed as:

$$c^{\text{water}} m^{\text{CHP}}_c (T^{\text{S}}_{c,n,t} - T^{\text{R}}_{c,n,t}) = H^{\text{CHP}}_{c,n,t} \quad \forall c \in C, \forall n \in N, \forall t \in T \tag{32}$$

$$P^{\text{pump}}_{q,n,t} = \frac{m^{\text{pump}}_q (Pr^{\text{S}}_{q,n,t} - Pr^{\text{R}}_{q,n,t})}{\eta^{\text{pump}}_q \rho} \quad \forall q \in Q, \forall n \in N, \forall t \in T \tag{33}$$

where c^{water} is the heat capacity of the liquid in the pipeline network of the heat station; m^{CHP}_c is the mass flow rate of the liquid in CHP system c; $T^{\text{S}}_{c,n,t}$ is the supply temperature of CHP system c at time t in scenario n; $T^{\text{R}}_{c,n,t}$ is the return temperature of CHP system c at time t in scenario n; m^{pump}_q is the mass flow rate of the liquid in pump q; $Pr^{\text{S}}_{q,n,t}$ is the supply pressure of pump q at time t in scenario n; $Pr^{\text{R}}_{q,n,t}$ is the return pressure of pump q at time t in scenario n; η^{pump}_q is the operating efficiency of pump q; and ρ is the density of the liquid in the pipeline.

2) Heat network constraints

The heat network constraints can be expressed as:

$$\begin{cases} \sum_{b^{\mathrm{h}} \in \Gamma_z^{\mathrm{pipe}-}} T_{b^{\mathrm{h}},n,t}^{\mathrm{SO}} m_{b^{\mathrm{h}},n,t}^{\mathrm{pipe}} = T_{z,n,t}^{\mathrm{S}} \sum_{b^{\mathrm{h}} \in \Gamma_z^{\mathrm{pipe}+}} m_{b^{\mathrm{h}},n,t}^{\mathrm{pipe}} \\ \sum_{b^{\mathrm{h}} \in \Gamma_z^{\mathrm{pipe}+}} T_{b^{\mathrm{h}},n,t}^{\mathrm{RO}} m_{b^{\mathrm{h}},n,t}^{\mathrm{pipe}} = T_{z,n,t}^{\mathrm{R}} \sum_{b^{\mathrm{h}} \in \Gamma_z^{\mathrm{pipe}-}} m_{b^{\mathrm{h}},n,t}^{\mathrm{pipe}} \quad \forall z \in Z, \forall n \in N, \forall t \in T \\ T_{b^{\mathrm{h}},n,t}^{\mathrm{SI}} = T_{z,n,t}^{\mathrm{S}} \quad \forall b^{\mathrm{h}} \in \Gamma_z^{\mathrm{pipe}-} \\ T_{b^{\mathrm{h}},n,t}^{\mathrm{RI}} = T_{z,n,t}^{\mathrm{R}} \quad \forall b^{\mathrm{h}} \in \Gamma_z^{\mathrm{pipe}+} \end{cases} \tag{34}$$

$$\begin{cases} T_{b^{\mathrm{h}},n,t}^{\mathrm{SO}} = (T_{b^{\mathrm{h}},n,t}^{\mathrm{SI}} - T_t^{\mathrm{am}}) \mathrm{e}^{-\frac{\lambda_{b^{\mathrm{h}}} L_{b^{\mathrm{h}}}}{c^{\mathrm{water}} m_{b^{\mathrm{h}},n,t}^{\mathrm{pipe}}}} + T_t^{\mathrm{am}} \quad \forall b^{\mathrm{h}} \in \Gamma_z^{\mathrm{pipe}-} \\ T_{b^{\mathrm{h}},n,t}^{\mathrm{RO}} = (T_{b^{\mathrm{h}},n,t}^{\mathrm{RI}} - T_t^{\mathrm{am}}) \mathrm{e}^{-\frac{\lambda_{b^{\mathrm{h}}} L_{b^{\mathrm{h}}}}{c^{\mathrm{water}} m_{b^{\mathrm{h}},n,t}^{\mathrm{pipe}}}} + T_t^{\mathrm{am}} \quad \forall b^{\mathrm{h}} \in \Gamma_z^{\mathrm{pipe}+} \end{cases} \quad \forall n \in N, \forall t \in T \tag{35}$$

where $\Gamma_z^{\mathrm{pipe}-}$ is the set of pipelines that end at node z; $T_{b^{\mathrm{h}},n,t}^{\mathrm{SO}}$ is the outlet temperature of the supply pipeline b^{h} at time t in scenario n; $m_{b^{\mathrm{h}},n,t}^{\mathrm{pipe}}$ is the water mass of the supply pipeline b^{h} at time t in scenario n; $T_{z,n,t}^{\mathrm{S}}$ is the supply temperature of heat network node z at time t in scenario n; $\Gamma_z^{\mathrm{pipe}+}$ is the set of pipes that begin at node z; $T_{b^{\mathrm{h}},n,t}^{\mathrm{RO}}$ is the outlet temperature of the return pipeline b^{h} at time t in scenario n; $T_{z,n,t}^{\mathrm{R}}$ is the return temperature of heat network node z at time t in scenario n; $T_{b^{\mathrm{h}},n,t}^{\mathrm{SI}}$ is the inlet temperature of the supply pipeline b^{h} at time t in scenario n; $T_{b^{\mathrm{h}},n,t}^{\mathrm{RI}}$ is the inlet temperature of the return pipeline b^{h} at time t in scenario n; T_t^{am} is the ambient temperature at time t; $\lambda_{b^{\mathrm{h}}}$ is the heat conductivity of pipeline b^{h}; and $L_{b^{\mathrm{h}}}$ is the length of pipeline b^{h}.

3) Heat exchange station constraint

The heat exchange station constraint can be expressed as:

$$c^{\mathrm{water}} m_z^{\mathrm{node}} (T_{z,n,t}^{\mathrm{S}} - T_{z,n,t}^{\mathrm{R}}) + H_{z,n,t}^{\mathrm{nsh}} = H_{z,n,t}^{\mathrm{node}} \quad \forall z \in Z, \forall n \in N, \forall t \in T \tag{36}$$

where m_z^{node} is the mass flow rate of the liquid at node z; and $H_{z,n,t}^{\mathrm{node}}$ is the predicted value of the heat load of node z at time t in scenario n.

3) NGS Operational Constraints

In deterministic scenario n, the NGS operational constraints include nodal flow balance and natural gas pipeline operational constraints [30].

1) Nodal flow balance constraint

The nodal flow balance constraint can be expressed as:

$$\sum_{s \in \Omega_a^{\mathrm{S}}} G_{s,n,t}^{\mathrm{sourse}} + \sum_{u \in \Omega_a^{\mathrm{U}}} G_{u,n,t}^{\mathrm{P2G}} + \sum_{b^{\mathrm{g}} \in \Omega_a^{\mathrm{g}+}} G_{b^{\mathrm{g}},n,t}^{\mathrm{pipe}} - \sum_{b^{\mathrm{g}} \in \Omega_a^{\mathrm{g}-}} G_{b^{\mathrm{g}},n,t}^{\mathrm{pipe}} + G_{a,n,t}^{\mathrm{ng}} = G_{a,n,t}^{\mathrm{load}} + \sum_{c \in \Omega_a^{\mathrm{C}}} G_{c,n,t}^{\mathrm{CHP}} + \sum_{r \in \Omega_a^{\mathrm{R}}} G_{r,n,t}^{\mathrm{gas\_turbine}} \quad \forall a \in A, \forall t \in T, \forall n \in N \tag{37}$$

where Ω_a^{S} is the set of natural gas sources connected to node a; $G_{s,n,t}^{\mathrm{sourse}}$ is the output of natural gas source s at time t in scenario n; Ω_a^{U} is the set of P2G systems connected to node a; $G_{u,n,t}^{\mathrm{P2G}}$ is the gas production of P2G system u at time t in scenario n; $\Omega_a^{\mathrm{g}+}$ is the set of the pipelines that begin at node a; $\Omega_a^{\mathrm{g}-}$ is the set of the pipelines that end at node a; $G_{b^{\mathrm{g}},n,t}^{\mathrm{pipe}}$ is the gas flow rate of natural gas network pipeline b^{g} at time t in scenario n; $G_{a,n,t}^{\mathrm{ng}}$ is the shed gas load of node a at time t in scenario n; $G_{a,n,t}^{\mathrm{load}}$ is the predicted gas load of node a at time t in scenario n; Ω_a^{C} is the set of CHP systems connected to node a; $G_{c,n,t}^{\mathrm{CHP}}$ is the gas consumption of CHP system c at time t in scenario n; Ω_a^{R} is the set of gas turbines connected to node a; and $G_{r,n,t}^{\mathrm{gas\_turbine}}$ is the gas consumption of gas turbine r at time t in scenario n.

2) Natural gas pipeline operational constraints

The natural gas pipeline operational constraints can be expressed as:

$$\left(\frac{\pi}{4}\right)^2 J_{b^{\mathrm{g}}} (p_{a,n,t}^2 - p_{b,n,t}^2) = G_{b^{\mathrm{g}},n,t}^{\mathrm{pipe}} \left| G_{b^{\mathrm{g}},n,t}^{\mathrm{pipe}} \right| \quad \forall b^{\mathrm{g}} \in \Omega^{\mathrm{g}}, \forall a \in \Omega_{b^{\mathrm{g}}}^{\mathrm{g}+}, \forall b \in \Omega_{b^{\mathrm{g}}}^{\mathrm{g}-}, \forall n \in N, \forall t \in T \tag{38}$$

$$-G_{b^{\mathrm{g}}}^{\max} \le G_{b^{\mathrm{g}},n,t}^{\mathrm{pipe}} \le G_{b^{\mathrm{g}}}^{\max} \quad \forall b^{\mathrm{g}} \in \Omega^{\mathrm{g}}, \forall n \in N, \forall t \in T \tag{39}$$

$$p_a^{\min} \le p_{a,n,t} \le p_a^{\max} \quad \forall a \in \Omega_{b^{\mathrm{g}}}^{\mathrm{g}+}, \forall n \in N, \forall t \in T \tag{40}$$

$$p_b^{\min} \le p_{b,n,t} \le p_b^{\max} \quad \forall b \in \Omega_{b^{\mathrm{g}}}^{\mathrm{g}-}, \forall n \in N, \forall t \in T \tag{41}$$

where $J_{b^{\mathrm{g}}}$ is the physical coefficient of natural gas pipeline b^{g}; $p_{a,n,t}$ is the pressure of node a at time t in scenario n; $p_{b,n,t}$ is the pressure of node b at time t in scenario n; Ω^{g} is the set of natural gas pipelines; $\Omega_{b^{\mathrm{g}}}^{\mathrm{g}+}$ is the set of first nodes of natural gas pipeline b^{g}; $\Omega_{b^{\mathrm{g}}}^{\mathrm{g}-}$ is the set of end nodes of natural gas pipeline b^{g}; $G_{b^{\mathrm{g}}}^{\max}$ is the upper limit of the gas flow rate of pipeline b^{g}; $p_a^{\min}$ and $p_a^{\max}$ are the lower and upper limits of the pressure at node a, respectively; and $p_b^{\min}$ and $p_b^{\max}$ are the lower and upper limits of the pressure at node b, respectively.

3) Model transformation

Equation (38) contains the nonlinear terms $G_{b^{\mathrm{g}},n,t}^{\mathrm{pipe}} \left| G_{b^{\mathrm{g}},n,t}^{\mathrm{pipe}} \right|$, $p_{a,n,t}^2$, and $p_{b,n,t}^2$, which lead to difficulties in the solution procedures. To solve this problem, an incremental linearization method [15] is employed to transform the original nonlinear optimization problem into a mixed-integer linear programming model that can be solved more efficiently.

4) Energy-coupling Device Operational Constraints

1) P2G system operational constraints

The P2G system operational constraints can be expressed by:

$$\begin{cases} G_{u,n,t}^{\mathrm{P2G}} = \eta_u^{\mathrm{P2G}} P_{u,n,t}^{\mathrm{P2G}} \\ M_{u,n,t}^{P2G} = \sum_{u \in U} \tau_u^{\mathrm{P2G}} P_{u,n,t}^{\mathrm{P2G}} \end{cases} \quad \forall u \in U, \forall n \in N, \forall t \in T \tag{42}$$

where η_u^{P2G} is the efficiency of P2G system u.

2) Gas turbine operational constraint

The gas turbine operational constraint can be expressed by:

$$P_{r,n,t}^{\mathrm{gas\_turbine}} = \eta_r^{\mathrm{gas\_turbine}} G_{r,n,t}^{\mathrm{gas\_turbine}} \quad \forall r \in R, \forall n \in N, \forall t \in T \tag{43}$$

where $\eta_r^{\mathrm{gas\_turbine}}$ is the efficiency of gas turbine r.

3) CHP system operational constraints

The CHP system operational constraints can be expressed as:

$$\begin{cases} P_{c,n,t}^{\mathrm{CHP}} = k_c^{\mathrm{CHP}} H_{c,n,t}^{\mathrm{CHP}} \\ G_{c,n,t}^{\mathrm{CHP}} = \dfrac{P_{c,n,t}^{\mathrm{CHP}} + H_{c,n,t}^{\mathrm{CHP}}}{k_c^{\mathrm{CHP}}} \end{cases} \quad \forall n \in N, \forall t \in T \tag{44}$$

where k_c^{CHP} is the efficiency of CHP system c.

V. Case Studies

Two test systems are employed to verify the effectiveness of the proposed method. One is the E14-H6-G6 system, which consists of a 14-node electric network, a 6-node heat network, and a 6-node gas network. The other is the E57-H12-G12 system, which consists of a 57-node electric network, a 12-node heat network, and a 12-node gas network. The topologies of the two test systems are shown in Supplemental Material A Fig. SA3 and Fig. SA4. The parameters of the electric network are referenced in [31] and [32], and the heat and gas network parameters are presented in [33]. MATLAB is used to call the GUROBI solver for solving the model. The computer is employed with a Windows 10 system, a 3.9 GHz Intel i5-8300H CPU, and 16 GB RAM. The total dispatching horizon is 24 hours.

A. E14-H6-G6 System

1) Analysis of Effectiveness of CCS-P2G Synergistic Operation Mode

To verify the effectiveness of the proposed CCS-P2G synergistic operation mode, comparative experiments are employed using the IES operation modes proposed in [3] and [34]. Three distinct scenarios are defined as follows.

Scenario 1: no coal-fired units are equipped with CCS system [3].

Scenario 2: some of the coal-fired units are equipped with CCS, but the CCS and P2G systems operate in the separate mode [34].

Scenario 3: some of the coal-fired units are equipped with CCS system, and the CCS and P2G systems operate in the synergistic operation mode.

1) Effects of carbon purchase costs of P2G systems

The coal-fired units described in Scenario 1 are not equipped with CCS system; therefore, the P2G systems cannot use the carbon emission from the coal-fired units for the methanation reaction and must purchase CO_2. As a result, the CO_2 purchase cost coefficient of P2G may affect the dispatch results. Therefore, we discuss the wind power accommodation capabilities and operating economy of the system under different CO_2 purchase cost coefficients. The total operating costs and the wind power accommodation rate of the IES with the CO_2 purchase cost coefficients are shown in Fig. 3.

As Fig. 3 shows, when the CO_2 purchase cost coefficient of P2G systems is 200 ¥/MWh or greater, the wind power accommodation rate is 70%, which is the same as when P2G systems are not in operation. Simultaneously, the operating cost of the IES reaches its peak at ¥7867.20×10^3. This is because with the increase in CO_2 purchase cost coefficients, the total revenue obtained by P2G systems to generate natural gas through the methanation reaction cannot cover the cost of purchasing CO_2, and using P2G systems for wind power accommodation is not economical. Therefore, P2G systems are out of operation. By contrast, with a decrease in the CO_2 purchase cost, the revenue obtained from using P2G systems for wind power accommodation, and the generated natural gas supplied to the gas network gradually increases. When the CO_2 purchase cost coefficient is 0 ¥/MWh, wind power cannot be fully accommodated due to the limitation of the P2G system capacity, and the highest wind power accommodation rate is 96.37%. Thus, CO_2 purchase cost coefficients and the capacities of P2G systems clearly have significant effects on the amount of wind power accommodation and the operating economics of the IES. In addition, sufficient CO_2 for P2G systems can be produced by coal-fired units equipped with CCS system, which effectively reduces the CO_2 purchase cost coefficients of P2G systems and increases the low-carbon economics of the IES.

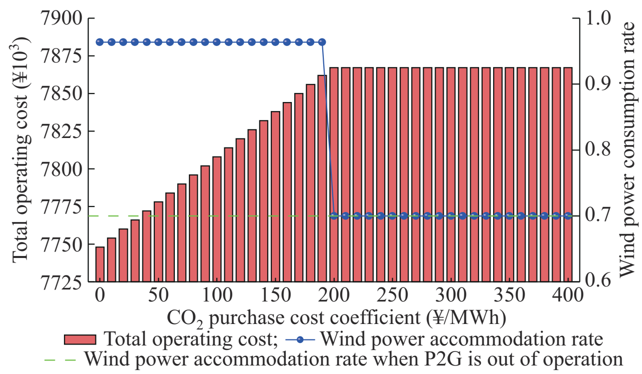

Fig. 3. Effects of CO_2 purchase costs of P2G systems on operating costs and wind power accommodation rate.

2) Dispatch results in different scenarios

The total cost of the IES as well as the fuel cost of coal-fired units, the cost of carbon trading, and the CO_2 purchase cost for P2G systems are compared in the three scenarios to further analyze the effect of CCS systems on IES low-carbon dispatch and to verify the effectiveness of the proposed CCS-P2G synergistic operation mode. The results are summarized in Table I.

TABLE I
Cost Comparisons of Three Scenarios

Scenario	Fuel cost of coal-fired units (¥10^3)	Carbon emission cost (¥10^3)	Carbon transportation cost (¥10^3)	CO_2 purchase cost for P2G (¥10^3)	Total cost (¥10^3)
1	1307.79	302.17	0	4.72	7444.97
2	1410.45	80.21	40.77	3.07	7375.76
3	1514.26	–59.71	35.91	0	7315.52

As Table I shows, the carbon emission cost in scenario 2 is ¥80.21×10^3, which is 73.46% less than that in scenario 1 because the carbon emission of coal-fired units with CCS system has decreased significantly. In terms of the fuel cost of the coal-fired units, the integration of CCS systems causes additional energy consumption of the coal-fired units.

Therefore, the fuel cost of the coal-fired units in scenario 2 increases by 7.8% over that in scenario 1. Carbon transportation costs occur in scenario 2 because the CO_2 captured by the CCS system must be transported and stored. In terms of the CO_2 purchase cost for P2G systems, because the energy consumption of CCS system can relieve the pressure of wind power accommodation on P2G systems, the CO_2 purchase cost for P2G systems in scenario 2 decreases by 35.10% as compared with that in scenario 1, and the total cost decreases by ¥69.22×10^3.

In scenario 3, the CCS-P2G synergistic operation mode is formulated based on scenario 2. The carbon emission cost is further reduced because the CO_2 captured by the CCS system is fully utilized. Because surplus carbon emission allowances can be sold in the carbon market, a profit of ¥59.71×10^3 is earned. In the CCS-P2G synergistic operation mode, as sufficient CO_2 captured by the CCS system can be directly supplied to P2G systems for the methanation reaction, the total amount of CO_2 required is reduced; the carbon transportation cost decreases by 11.92%; and the CO_2 purchase cost for P2G systems is reduced to zero. As a result, the total operating cost is ¥60.24×10^3 less than that in scenario 2 and ¥129.46×10^3 less than that in scenario 1. Thus, the proposed CCS-P2G synergistic operation mode significantly improves the operational economy and low-carbon performance of the IES through the full reuse of CO_2, thus verifying the effectiveness of the CCS-P2G synergistic operation mode in low-carbon dispatch.

2) Results of ECEF

To verify the effectiveness of the proposed ECEF model when considering the ESS, three typical periods are selected in scenario 3: 01:00-02:00, which is the period of the wind power peak and load valley; 14:00-15:00, which is the load valley period; and 18:00-19:00, which is the period of the load peak and wind power valley.

Table II lists the power outputs of devices during these periods, and Supplemental Material C Fig. SC1 shows the CEF.

TABLE II
POWER OUTPUTS OF DEVICES DURING TYPICAL PERIODS

Period	$P^{\text{P2G}}_{u,n,t}$ (MW)	$P^{\text{cha}}_{e,n,t}$(MW)	$P^{\text{dis}}_{e,n,t}$(MW)	$P^{\text{external\_grid}}_{o,n,t}$ (MW)	$P^{\text{f}}_{w,n,t}$ (MW)
01:00-02:00	−100.00	−40.00	0	−60.00	184.00
14:00-15:00	0	−59.97	0	−60.00	38.00
18:00-19:00	0	0	19.68	−60.00	35.00

According to Supplemental Material C Fig. SC1(a) and Fig. SC1(d), during 01:00-02:00, the overall direction of the CEF exhibits a trend of spreading from node 14, which is connected to the wind turbine, to the entire network. A high proportion of wind power reduces the NCI of the entire network while increasing the pressure on the system to accommodate wind power. The P2G systems use surplus wind power to produce natural gas to avoid penalty costs caused by wind curtailment. The problem of wind power accommodation has also been effectively solved while reducing the gas production cost of the gas source. Due to the green power provided by wind power, the NCI of node 14 decreases to zero. According to constraint (14) of the ECEF model, when the NCI of the node connected to the ESS decreases to zero, the electricity stored by the ESS contains no carbon emission, thus realizing the flexible utilization of low-carbon resources. Supplemental Material C Fig. SC1(f) shows that the injection of low-carbon wind power reduces the SOCB of the ESS, which is equivalent to using low-carbon wind power to reduce the original high-carbon electricity in the ESS so that the carbon emission per unit of electric energy is reduced. In subsequent dispatching, the ESS can reduce the NCI of the entire network while meeting the load demand by releasing low-carbon electric energy, thereby achieving low-carbon operation of the system.

Supplemental Material C Fig. SC1(b) and Fig. SC1(d) reveal that during 14:00-15:00, which is the valley of wind power, the overall direction of the CEF shows a trend of spreading from node 13, which is connected to the gas turbine, to the entire network. Due to the increase in the proportion of output from high-carbon-emission units, the NCIs of all nodes in the network increase compared with the value during 01:00-02:00. The NCI of node 14 with the ESS increases from 0 gCO_2/kWh to 286.34 gCO_2/kWh. To ensure the global optimality of the dispatch decision, the ESSs are charged during 14:00-15:00 to meet the energy demand in subsequent electrical load peak periods. According to constraint (14), because the NCI of the node where the ESS is located is not zero, the electric energy containing carbon emission is charged to the ESS, which causes an upward trend in the SOCB of the ESSs during 14:00-15:00, as shown in Supplemental Material C Fig. SC1(f).

Supplemental Material C Fig. SC1(c) and Fig. SC1(d) show that during 18:00-19:00, which is the peak of electrical load, the wind power accommodation rate further decreases, and to ensure the global optimality of the dispatching decision, the ESS is discharged to meet the load demand. At this time, the SOCB of the ESS is 0.26 tCO_2/MWh. The ECEF model shows that when the ESS is in the discharging state, it is equivalent to special power-generation device, and the SOCB of the ESS is the GCI of this special power-generation device. A limited amount of low-carbon electric released by the ESS is injected into the grid to reduce the NCIs of some nodes. The NCI of node 9 is lower than that during 14:00-15:00 due to the proximity of node 14 in its connection to the ESS. This means that the ESS realizes the flexible use of low-carbon resources through the storage of wind power and improves the low-carbon economy of the IES operation.

As Fig. 4 shows, during the low-electrical load periods from 14:00 to 17:00, the carbon emissions released from the generator side are higher than those absorbed from the load side. Excess carbon emission is then attached to electrical energy and charged into the ESS. During the electrical load peak periods from 10:00 to 13:00 and from 18:00 to 21:00, the carbon emissions flowing into the loads are greater than those released from the generators, and the shortage is supplemented by the carbon-containing electricity released from the ESS. Thus, in the proposed ECEF model under the regulation of the ESS, the real-time balance of carbon supply and demand is broken and then shifts to the carbon emission in the entire dispatch horizon.

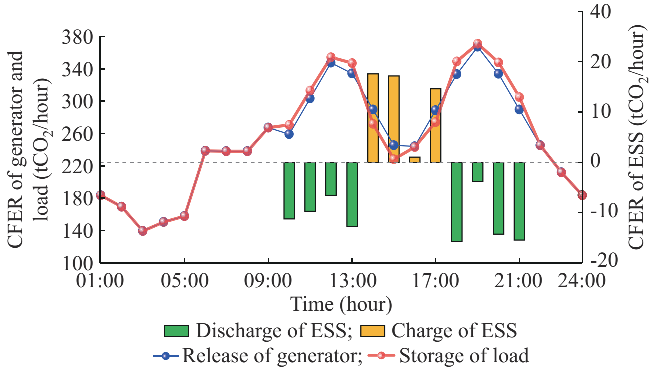

Fig. 4. CEF differences between supply and demand sides.

We can conclude that the proposed ECEF model with an ESS can accurately describe the flow path of the carbon emission in an IES. It also clarifies that the ESS can flexibly use low-carbon resources. The proposed ECEF model is an effective tool for formulating and analyzing low-carbon dispatch strategies.

3) Effectiveness of PMADP Algorithm

Low-carbon economic dispatching of an IES with multivariate uncertainty is a multidimensional dynamic planning problem that encounters the subproblems of high time consumption and "curse of dimensionality". In this study, the PMADP algorithm is used to alleviate the "curse of dimensionality" problem by state variable aggregation, state space compression, and parallel computing without loss of accuracy. To verify the effectiveness of the PMADP algorithm in solving the low-carbon economic dispatch problem with multivariate uncertainty, the solution accuracy and efficiency of the traditional stochastic optimization algorithm and serial multi-dimensional approximate dynamic programming (MADP) algorithm are compared with those of the PMADP algorithm used in this study, with the results listed in Table III.

TABLE III
COMPARISONS OF DIFFERENT ALGORITHMS

Algorithm	Cost expectation (¥10^3)	Total time consumed (s)
Stochastic optimization	7350.77	4209.21
MADP	7410.19	862.40
PMADP	7410.19	408.91

Table III shows that in terms of cost expectation, the stochastic optimization algorithm obtains the lowest cost of ¥7350.77×10^3 by solving each scenario exactly. The traditional serial MADP algorithm and parallelized PMADP algorithm used in this study approximate the value function to alleviate the "curse of dimensionality", and the cost expectation is slightly increased by 0.81% compared with that of the stochastic optimization algorithm. In terms of time consumption, the PMADP algorithm utilizes computational resources in a parallel manner by decoupling serial tasks and requires the shortest time among the three algorithms, specifically, 90.29% and 52.58% less time than those of the stochastic optimization and traditional serial MADP algorithms, respectively.

In summary, although the stochastic optimization algorithm can solve each scene precisely, its low efficiency limits its application to large-scale systems. The traditional serial MADP algorithm shows an improvement in terms of computational efficiency compared with that of the stochastic optimization algorithm. However, its insufficient utilization of computational resources limits its application in practical engineering. The PMADP algorithm used in this study not only maintains the calculation accuracy, but also significantly improves the computational efficiency by fully using the computational resources.

B. E57-H12-G12 System

To further verify the applicability of the proposed ECEF model to large-scale systems, we conducted a test on a modified IEEE 57-bus system with two sets of wind turbines and ESSs. We select the three typical time periods used in the E14-H6-G6 system and use the proposed ECEF model to analyze the characteristics of carbon emission during each period. The results are shown Supplemental Material D Fig. SD1.

Supplemental Material D Fig. SD1(a) shows that during 01:00-02:00, the green wind power spreads to the perimeter from connected nodes 33 and 57, reducing the NCIs of its adjacent nodes to 0. The ESS stores clean electricity without carbon emission to achieve coordinated utilization of low-carbon resources during different periods. An examination of the change in the SOCB of the ESS in Supplemental Material D Fig. SD1(f) reveals that during the wind power output peak and load valley period of 01:00-02:00, because of the injection of low-carbon wind power, the SOCBs of the two ESSs significantly decrease. The ESSs reduce their internal "carbon concentration" by storing low-carbon electricity, and in the subsequent dispatch process, low-carbon resources are flexibly utilized to achieve low-carbon and economical system operation.

Supplemental Material D Fig. SD1(b) shows that during the wind power valley period of 14:00-15:00, the proportion of output power from the coal-fired units increases, which causes the NCIs of all nodes in the network to increase. The NCIs of nodes 33 and 57 where the ESSs are connected increase from 0 gCO_2/kWh to 122.18 gCO_2/kWh and 125.41 gCO_2/kWh, respectively. Supplemental Material D Fig. SD1(f) shows that in the ECEF model, because of the non-zero NCI of the node that connects with the ESS, the carbon electricity is injected into the charging process of the ESS during the low-load period, and the "carbon concentration" of the ESS increases accordingly. Therefore, SOCB shows an increasing trend during 14:00-15:00.

Supplemental Material D Fig. SD1(c) shows that the ESS discharges to meet the load demand during 18: 00-19: 00, which is the peak hour of the electrical load. In the ECEF model proposed in this study, the SOCB of the ESS during discharging process determines the GCI of the node where the ESS is located. During 18:00-19:00, the SOCB values of the two ESSs are 0.11 and 0.12 tCO_2/MWh, respectively. Low-carbon electricity is injected into the electric network during the ESS discharging process. Flexible utilization of low-carbon resources reduces the NCI, which contributes to the low-carbon operation of the system.

The aforementioned results show that even in a system with multiple ESSs, the ECEF model proposed in this study could still accurately depict the process of carbon emission and calculate the SOCB of ESSs throughout the entire dispatch cycle, thus enabling a clear demonstration of the flexible utilization of low-carbon energy and its penetration range.

VI. Conclusion

In this study, a CCS-P2G synergistic operation mode and a low-carbon dispatch model based on ECEF are proposed, and the following conclusions are drawn.

1) The CCS-P2G synergistic operation mode, which integrates carbon emission generation, capture, and utilization reuses the emitted carbon and contributes to the low-carbon operation of the system.

2) By tracking the carbon emission process of ESS over the entire dispatch horizon, the role of ESSs in low-carbon dispatch is clarified, thus improving the accuracy and rationality of the low-carbon dispatch strategy of IES.

3) The proposed ECEF model with ESSs considered can accurately describe the CEF process of a system with ESSs, enabling perspective shift from energy to carbon, thus providing an evaluation approach for low-carbon scheduling strategies. The ECEF model can also be applied to large-scale systems that consist of multiple ESSs.

References

[1] Y. Yu, X. Han, M. Yang *et al*., "Probabilistic prediction of regional wind power based on spatiotemporal quantile regression," *IEEE Transactions on Industry Applications*, vol. 56, no. 6, pp. 6117-6127, Nov. 2020.

[2] X. Zhang, Y. Zhang, X. Ji *et al*., "Unit commitment of integrated energy system considering conditional value-at-risk and P2G," *Electric Power Systems Research*, vol. 221, p. 109398, Aug. 2023.

[3] Y. Zhang, Y. Han, D. Liu *et al*., "Low-carbon economic dispatch of electricity-heat-gas integrated energy systems based on deep reinforcement learning," *Journal of Modern Power Systems and Clean Energy*, vol. 11, no. 4, pp. 1827-1841, Nov. 2023.

[4] Y. Zhang, X. Zhang, X. Ji *et al*., "Optimization of integrated energy system considering transmission and distribution network interconnection and energy transmission dynamic characteristics," *International Journal of Electrical Power & Energy Systems*, vol. 153, p. 109357, Nov. 2023.

[5] Z. Ma, Y. Zhou, Y. Zheng *et al*., "Distributed robust optimal dispatch of regional integrated energy systems based on ADMM algorithm with adaptive step size," *Journal of Modern Power Systems and Clean Energy*, vol. 12, no. 3, pp. 852-862, May 2024.

[6] Z. Li, L. Wu, Y. Xu *et al*., "Multi-stage real-time operation of a multi-energy microgrid with electrical and heat energy storage assets: a data-driven MPC-ADP approach," *IEEE Transactions on Smart Grid*, vol. 13, no. 1, pp. 213-226, Jan. 2022.

[7] J. Li, G. Li, S. Ma *et al*., "Modeling and simulation of hydrogen energy storage system for power-to-gas and gas-to-power systems," *Journal of Modern Power Systems and Clean Energy*, vol. 11, no. 3, pp. 885-895, May 2023.

[8] Y. Jiang, C. Wan, A. Botterud *et al*., "Efficient robust scheduling of integrated electricity and heat systems: a direct constraint tightening approach," *IEEE Transactions on Smart Grid*, vol. 12, no. 4, pp. 3016-3029, Jul. 2021.

[9] P. Li, F. Zhang, X. Ma *et al*., "Operation cost optimization method of regional integrated energy system in electricity market environment considering uncertainty," *Journal of Modern Power Systems and Clean Energy*, vol. 11, no. 1, pp. 368-380, Jan. 2023.

[10] F. Liu, Z. Bie, and X. Wang, "Day-ahead dispatch of integrated electricity and natural gas system considering reserve scheduling and renewable uncertainties," *IEEE Transactions on Sustainable Energy*, vol. 10, no. 2, pp. 646-658, Apr. 2019.

[11] J. Tan, Q. Wu, Q. Hu *et al*., "Adaptive robust energy and reserve co-optimization of integrated electricity and heat system considering wind uncertainty," *Applied Energy*, vol. 260, p. 114230, Feb. 2020.

[12] P. Li, Z. Wang, J. Wang *et al*., "Two-stage optimal operation of integrated energy system considering multiple uncertainties and integrated demand response," *Energy*, vol. 225, p. 120256, Jun. 2021.

[13] G. Li, R. Zhang, T. Jiang *et al*., "Security-constrained bi-level economic dispatch model for integrated natural gas and electricity systems considering wind power and power-to-gas process," *Applied Energy*, vol. 194, pp. 696-704, May 2017.

[14] J. Duan, Y. Yang, and F. Liu, "Distributed optimization of integrated electricity-natural gas distribution networks considering wind power uncertainties," *International Journal of Electrical Power & Energy Systems*, vol. 135, p. 107460, Feb. 2022.

[15] Z. Zhang, C. Wang, H. Lv *et al*., "Day-ahead optimal dispatch for integrated energy system considering power-to-gas and dynamic pipeline networks," *IEEE Transactions on Industry Applications*, vol. 57, no. 4, pp. 3317-3328, Jul. 2021.

[16] L. Zhang, D. Liu, G. Cai *et al*., "An optimal dispatch model for virtual power plant that incorporates carbon trading and green certificate trading," *International Journal of Electrical Power & Energy Systems*, vol. 144, p. 108558, Jan. 2023.

[17] Y. Xiang, G. Wu, X. Shen *et al*., "Low-carbon economic dispatch of electricity-gas systems," *Energy*, vol. 226, p. 120267, Jul. 2021.

[18] Q. Tan, Y. Ding, Q. Ye *et al*., "Optimization and evaluation of a dispatch model for an integrated wind-photovoltaic-heat power system based on dynamic carbon emission trading," *Applied Energy*, vol. 253, p. 113598, Nov. 2019.

[19] F. Yu, X. Chu, D. Sun *et al*., "Low-carbon economic dispatch strategy for renewable integrated power system incorporating carbon capture and storage technology," *Energy Reports*, vol. 8, pp. 251-258, Nov. 2022.

[20] L. He, Z. Lu, L. Geng *et al*., "Environmental economic dispatch of integrated regional energy system considering integrated demand response," *International Journal of Electrical Power & Energy Systems*, vol. 116, p. 105525, Mar. 2020.

[21] D. Yang, Y. Xu, X. Liu *et al*., "Economic-emission dispatch problem in integrated electricity and heat system considering multi-energy demand response and carbon capture technologies," *Energy*, vol. 253, p. 124153, Aug. 2022.

[22] A. Akbari-Dibavar, B. Mohammadi-Ivatloo, K. Zare *et al*., "Economic-emission dispatch problem in power systems with carbon capture power plants," *IEEE Transactions on Industry Applications*, vol. 57, no. 4, pp. 3341-3351, Jul. 2021.

[23] Y. Wang, J. Qiu, Y. Tao *et al*., "Low-carbon oriented optimal energy dispatch in coupled natural gas and electricity systems," *Applied Energy*, vol. 280, p. 115948, Dec. 2020.

[24] Y. Cheng, N. Zhang, B. Zhang *et al*., "Low-carbon operation of multiple energy systems based on energy-carbon integrated prices," *IEEE Transactions on Smart Grid*, vol. 11, no. 2, pp. 1307-1318, Mar. 2020.

[25] C. Kang, T. Zhou, Q. Chen *et al*., "Carbon emission flow in networks," *Scientific Reports*, vol. 2, p. 479, 2012.

[26] C. Kang, T. Zhou, Q. Chen *et al*., "Carbon emission flow from generation to demand: a network-based model," *IEEE Transactions on Smart Grid*, vol. 6, no. 5, pp. 2386-2394, Sept. 2015.

[27] Y. Cheng, N. Zhang, Y. Wang *et al*., "Modeling carbon emission flow in multiple energy systems," *IEEE Transactions on Smart Grid*, vol. 10, no. 4, pp. 3562-3574, Jul. 2019.

[28] L. He, Z. Lu, J. Zhang *et al*., "Low-carbon economic dispatch for electricity and natural gas systems considering carbon capture systems and power-to-gas," *Applied Energy*, vol. 224, pp. 357-370, Aug. 2018.

[29] Z. Ji, C. Kang, Q. Chen *et al*., "Low-carbon power system dispatch incorporating carbon capture power plants," *IEEE Transactions on Power Systems*, vol. 28, no. 4, pp. 4615-4623, Nov. 2013.

[30] M. Cao, C. Shao, B. Hu *et al*., "Reliability assessment of integrated energy systems considering emergency dispatch based on dynamic optimal energy flow," *IEEE Transactions on Sustainable Energy*, vol. 13, no. 1, pp. 290-301, Jan. 2022.

[31] B. Liu, F. Liu, B. Zhai *et al*., "Investigating continuous power flow solutions of IEEE 14-bus system," *IEEJ Transactions on Electrical and Electronic Engineering*, vol. 14, no. 1, pp. 157-159, Jan. 2019.

[32] P. K. Dhal and K. Ramash Kumar, "A novel hybrid particle swarm-multiverse optimization based voltage stability improvement in IEEE

57 bus system," *International Journal of Engineering & Technology*, vol. 7, no. 2.24, p. 381, Apr. 2018.

[33] X. Chen, C. Wang, Q. Wu *et al*., "Optimal operation of integrated energy system considering dynamic heat-gas characteristics and uncertain wind power," *Energy*, vol. 198, p. 117270, May 2020.

[34] A. Akbari-Dibavar, B. Mohammadi-Ivatloo, K. Zare *et al*., "Economic-emission dispatch problem in power systems with carbon capture power plants," *IEEE Transactions on Industry Applications*, vol. 57, no. 4, pp. 3341-3351, Jul. 2021.

Yumin Zhang received the Ph.D. degree from Shandong University, Jinan, China, in 2019. She conducted post-doctoral research with the School of Electrical Engineering of Shandong University from November 2022 to November 2024. She is currently an Associate Professor at the College of Electrical Engineering and Automation, Shandong University of Science and Technology, Qingdao, China. Her research interests include power system operation and control, integrated energy system, renewable energy, low-carbon electricity technology, electricity market, wind power forecasting and artificial intelligence techniques.

Pengkai Sun received the B.E. degree in electrical engineering and automation from Shandong University of Science and Technology, Qingdao, China, in 2020. Currently, he is pursuing the M.Eng. degree in Shandong University of Science and Technology. His research interest focuses on power system operation and control.

Xingquan Ji received the B.E. and M.E. degrees from Shandong University, Jinan, China, in 1994 and 1998, respectively, and the Ph.D. degree from Tianjin University, Tianjin, China, in 2002, all in electrical engineering. He conducted post-doctoral research with Zhejiang University, Hangzhou, China, from July 2003 to July 2005. He is currently a Professor at the College of Electrical Engineering and Automation, Shandong University of Science and Technology, Qingdao, China. His research interests include integrated energy system dispatch optimization, distribution network optimal operation, and electricity market.

Fushuan Wen received the B.E. and M.E. degrees from Tianjin University, Tianjin, China, in 1985 and 1988, respectively, and the Ph.D. degree from Zhejiang University, Hangzhou, China, in 1991, all in electrical engineering. He joined Zhejiang University as a Faculty Member in the School of Electrical Engineering, in 1991, where he has been a Full Professor since 1997. He has also been a Full Professor with the Hainan Institute, Zhejiang University, since 2022. He is a Visiting Principal Research Scientist in Shenzhen Institute of Artificial Intelligence and Robotics for Society, Shenzhen, China, and the Director of Sanya Global Energy Research Institute, Sanya, China. He has been listed in "Most Cited Chinese Researchers" by Elsevier in eight consecutive years since 2015. He is the Editor-in-Chief of Energy Conversion and Economics (IET), the Deputy Editor-in-Chief of Automation of Electric Power Systems, and serves as the Editor, Subject Editor and Associate Editor of several international journals. His research interests include power industry restructuring, power system alarm processing, fault diagnosis and restoration strategies, smart grid and electric vehicle, as well as artificial intelligence application in power and integrated energy systems.

Ming Yang received the B.E. and Ph.D. degrees in electrical engineering from Shandong University, Jinan, China, in 2003 and 2009, respectively. He was an exchange Ph.D. student at the Energy System Research Center, University of Texas at Arlington, Arlington, USA, from October 2006 to October 2007. He conducted postdoctoral research at the School of Mathematics, Shandong University, from July 2009 to July 2011. From November 2015 to October 2016, he was a Visiting Scholar in the Energy Systems Division, Argonne National Laboratory, Argonne, USA. Currently, he is a Professor with Shandong University. His research interests include power system optimal operation and control.

Pingfeng Ye received the B.Eng. and Ph.D. degrees from Shandong University, Jinan, China, in 2011 and 2021, respectively. He is currently a Lecturer at the College of Energy Storage Technology, Shandong University of Science and Technology, Qingdao, China. His research interests include power system operation and control, and reactive power optimization.